

## Beta decay of $^{31,32}\text{Na}$ and $^{31}\text{Mg}$ : Study of the $N=20$ shell closure

G. Klotz, P. Baumann, M. Bounajma, A. Huck, A. Knipper, and G. Walter  
*Centre de Recherches Nucléaires, Université Louis Pasteur, F-67037 Strasbourg, France*  
*and the Isolde Collaboration, CERN, 1211 Geneva 23, Switzerland*

G. Marguier  
*Institut de Physique Nucléaire, Université Claude Bernard, F-69622 Villeurbanne, France*  
*and the Isolde Collaboration, CERN, 1211 Geneva 23, Switzerland*

C. Richard-Serre  
*Institut National de Physique Nucléaire et de Physique des Particules, F-75013 Paris, France*  
*and the Isolde Collaboration, CERN, 1211 Geneva 23, Switzerland*

A. Poves and J. Retamosa  
*Departamento de Física Teórica, C-XI, Universidad Autónoma, Cantoblanco, E-28049 Madrid, Spain*

(Received 21 December 1992)

The  $^{31,32}\text{Na}$  and  $^{31}\text{Mg}$  beta decays were studied at the CERN on-line mass separator ISOLDE by gamma, gamma-gamma, and neutron-gamma measurements. In the  $^{31}\text{Na}$  decay, the assignment of previously reported  $\gamma$  transitions and the observation of a new level at 3760 keV lead to a revised decay scheme which is found in good agreement with a calculation including two-particle-two-hole configurations in the model space, as far as only low-lying levels of  $^{31}\text{Mg}$  are concerned. In the  $^{31}\text{Mg} \rightarrow ^{31}\text{Al}$  decay, a new decay scheme involves ten  $\beta$  branches and three states are reported for the first time. While satisfactory agreement with theoretical calculations is observed for excitation energies in  $^{31}\text{Al}$ , a strong discrepancy is observed for the intensity of the ground-state  $\beta$  branch, the experimental one being highly quenched as compared to theoretical expectations. Finally, new spectroscopic results have been obtained in the  $^{32}\text{Na}$   $\beta$  decay. A previously noninterpreted 1436 keV  $\gamma$  ray is now assigned in the  $^{32}\text{Mg}$  scheme. The 240 keV ray is shown to arise from  $^{31}\text{Mg}$  produced in the one-neutron channel, and to be related to the decay of an intruder state at  $E_x = 461$  keV. The latter is partially fed from the 1390 keV level. Both nicely compare with theoretical predictions locating  $1\hbar\omega$  states at 0.40 MeV ( $\frac{7}{2}^-$ ) and 1.57 MeV ( $\frac{11}{2}^-$ ). The first experimental evidence for a  $\gamma$  cascade in the descendant  $^{32}\text{Al}$  is also obtained.

PACS number(s): 27.30.+t, 23.20.Lv, 21.10.Hw, 21.60.Cs

### I. INTRODUCTION

Studies of neutron-rich nuclei in the region around  $Z=11$ ,  $N=20$  have been initiated by the mass measurements of Na and Mg isotopes [1,2], indicating an excess in binding energy, and stimulated by the subsequent observation of a low-lying excited state in the even-even  $^{32}\text{Mg}$  isotope [3].

The experimental evidence for a region of strong deformation along a single closed shell has been augmented since then by additional results on neighboring nuclei and detailed comparisons with theoretical descriptions. When compared to shell model calculations, very successful for the  $N=18$  isotones, the  $N=20$  nuclei  $^{31}\text{Na}$  and  $^{32}\text{Mg}$  appeared incompatible with a shell model description [4]. Likewise, the  $^{31}\text{Mg}$  spectrum was found completely anomalous in the context of  $sd$ -shell systematics among the  $N=19$  isotones [5]. A better agreement with the experimental results was obtained by Hartree-Fock calculations on Na isotopes with contribution of the  $f_{7/2}$  orbit for the neutron [6] and by shell model calculations in the  $(sd, f)$  [7] or  $(sd, fp)$  [8] space.

The importance of the  $(sd)^{-2}(fp)^2$  neutron configurations in the low-energy states of  $N=20$  isotones was confirmed by the observation of the  $^{34}\text{Si}$  level scheme and its shell model interpretation with a mixed  $(0+2)\hbar\omega$

calculation [9].

Detailed discussions of the mechanisms responsible for the lowering of the  $2\hbar\omega$  excitation relative to  $0\hbar\omega$  and leading to a region of inversion around  $^{32}\text{Na}$  have been published recently [10–12]. In the study by Warburton *et al.* [10], calculations are made separately for the  $0\hbar\omega$  and  $2\hbar\omega$  excitations, the results of a weak-coupling model being used to relate the excitation energy of the  $n\hbar\omega$  configurations to the calculated  $0\hbar\omega$  binding energies. Good predictive power is obtained for binding energies of  $N \geq 20$  nuclei, apart from the fact that  $^{32,33}\text{Na}$  remain still underbound. When compared to the results of the mixed  $(0+2)\hbar\omega$  calculations [11,12], a general agreement is found with differences in the properties of excited states of  $N=19$  and 20 isotopes.

The existence of a deformed region, with coexisting spherical and deformed states at low energy for  $^{31}\text{Na}$ ,  $^{32}\text{Mg}$ ,  $^{33}\text{Al}$ , and  $^{34}\text{Si}$  has also been suggested by Heyde and Wood [13] using methods already applied to the evaluation of two-particle-two-hole (2p-2h) intruder excitations along single closed shells in different places of the nuclear mass table [14]. More recently, the strong deformation of several neutron-rich Na and Mg isotopes has been predicted by Patra and Prahara [15] using a relativistic mean-field model of interacting nucleons and mesons.

The experimental information on binding energies in the region around  $Z = 11$ ,  $N = 20$  is now well documented with new mass determinations [16–19]. On the contrary, the knowledge of excited states of  $N = 19, 20$  nuclei from previous  $\beta$ -decay [20] and multinucleon transfer reaction [21–23] studies is far from complete. More experimental data are needed in order to delineate the region of  $0\hbar\omega$  and  $2\hbar\omega$  inversion, locate the energies of intruder states, and extend the comparison with the calculations.

The present investigation of the  $^{31}\text{Na}$  decay was therefore undertaken to study the  $^{31}\text{Mg}$  isotope ( $N = 19$ ), which provides an interesting case for testing the predictions of models relative to  $0\hbar\omega$  and  $1\hbar\omega$  excitations. A return to the  $^{32}\text{Na}$  decay was also necessary because of the importance of the  $^{32}\text{Mg}$  level structure for the understanding of this region and the possibility to populate specific levels in  $^{31}\text{Mg}$  through the beta-delayed  $1n$  channel. To sort out experimental data, a reinvestigation of the  $\beta$  decay of  $^{31}\text{Mg}$  was necessary and it allowed the addition of spectroscopic information in the  $^{31}\text{Al}$  level scheme. This information is particularly valuable as the  $^{31}\text{Al}$  low-energy level scheme is perfectly reproduced in  $sd$ -shell model calculations, and contradictions for upper levels can reveal an anomaly in the  $N = 20$  shell closure. Preliminary results have been reported in Ref. [24].

The experimental conditions are first briefly described. The results obtained in the beta-decay studies of  $^{31}\text{Na}$ ,  $^{31}\text{Mg}$ , and  $^{32}\text{Na}$  are then presented. The shell model calculations and the theoretical predictions which can be compared to the measurements are discussed.

## II. EXPERIMENTAL METHODS

In our experiments, Na, Mg, and Al isotopes were produced by bombarding an uranium carbide target ( $\approx 15 \text{ g/cm}^2$ ) with  $2.0 \mu\text{A}$ ,  $600 \text{ MeV}$  protons from the CERN synchrocyclotron. These different atoms were ionized through surface ionization and mass separated in the ISOLDE 2 separator. Typical yields for  $^{31}\text{Na}$  ( $T_{1/2} = 17 \text{ ms}$ ) and  $^{32}\text{Na}$  ( $T_{1/2} = 14 \text{ ms}$ ) were 100 and 15 atoms/s, respectively. Magnesium and aluminum isotopes resulted either from radioactive decay or direct production from the source. In spite of the higher ionization potential and the lower volatility of these elements, their direct production from the target is observed when the ion source temperature is increased and this feature has been turned to account in previous studies [9,25].

The selected beams were collected on a moving tape system where suitable collection-counting cycles were chosen to optimize the observation. The setup included a thin NE102 plastic scintillator for beta detection (80% efficiency) at the collection point, two germanium gamma counters, and an efficient neutron detector consisting of three hexagonal cells each filled with  $3750 \text{ cm}^3$  NE213 liquid scintillator. This setup allowed us to perform  $\beta$ - $\gamma$ ,  $\beta$ - $\gamma$ - $\gamma$ , and  $\beta$ - $\gamma$ - $n$  measurements. Multiparametric events were registered on magnetic tape for subsequent analysis. A small  $\text{BaF}_2$  counter was also used to measure the lifetime of low-energy transitions.

## III. EXPERIMENTAL RESULTS

### A. Experimental $\beta$ decay of $^{31}\text{Na}$

Before the present work, information on the  $\beta$  decay of  $^{31}\text{Na}$  resulted from Ref. [20] and the studies quoted therein. From these investigations, we use the following important parameters: (i) half-life of  $17.0 \pm 0.4 \text{ ms}$  and (ii)  $P_{1n}$  and  $P_{2n}$  values  $37.3 \pm 5.4$  and  $0.87 \pm 0.24$ , respectively.

The estimated  $Q_\beta$  value of  $15.42 \pm 0.51 \text{ MeV}$  is a computed weighted average deduced from the mass excesses of  $^{31}\text{Na}$  and  $^{31}\text{Mg}$  given in a compilation [26] and in recent measurements at GANIL [18] and Los Alamos [19]. Although the origin of this parameter is different from that of the corresponding one in Ref. [20], the inferred results comes out at nearly the same value. The updated mass value  $Q_\beta$  is also used to calculate the one- and two-neutron separation energies in  $^{31}\text{Mg}$ , locating as a result the  $^{29}\text{Mg}$  and  $^{30}\text{Mg}$  excited level systems relatively to the  $^{31}\text{Mg}$  ground state. These are fed in the  $\beta$ -delayed one- and two-neutron processes.

TABLE I. Energy and intensity of  $\gamma$  rays observed in the  $\beta$  decay of  $^{31}\text{Na}$ .

$E_\gamma^a$ (keV)	$I_\gamma$ (relative)	$I_\gamma$ (per 100 decays)	Transition <sup>a</sup> (MeV)
50.5±0.7	125.4±15.5	19.5±3.9	0.050–0
54.6±0.1 <sup>b</sup>			0.055–0 <sup>c</sup>
170.5±0.5	35.0±2.0	5.4±0.9	0.22–0.050
221.0±0.5	14.2±1.1	2.2±0.4	0.22–0.050
305.6±0.3 <sup>d</sup>	13.6±1.3	2.0±0.7	1.79–1.48 <sup>d</sup>
451.1±1.1	2.9±0.8	0.4±0.1	0.67–0.22
622.6±1.4	23.0±1.8	3.6±0.6	0.67–0.050
673.1±1.2	11.6±0.9	1.8±0.3	0.67–0
807.6±0.6	9.4±1.4	1.5±0.3	1.03–0.22
894.6±0.7	5.8±1.2	0.9±0.2	0.94–0.050
985.1±0.4 <sup>d</sup>	12.0±2.2 <sup>c</sup>	1.8±0.7	2.47–1.48 <sup>d</sup>
1039.9±0.2 <sup>c</sup>	0.20±0.06	0.03±0.01	1.09–0.055 <sup>c</sup>
1214.7±0.9	10.0±1.0	1.6±0.3	2.24–1.03
1482.0±0.3 <sup>d</sup>	100	15.0±5.0	1.48–0 <sup>d</sup>
1571.1±1.2	16.8±1.9	2.6±0.5	3.81–2.24
1638.0±0.2 <sup>c</sup>	0.10±0.04	0.02±0.01	1.64–0 <sup>c</sup>
1820.2±0.6 <sup>d</sup>	20.0±2.2 <sup>c</sup>	3.0±1.0	1.82–0 <sup>d</sup>
1978.0±0.6 <sup>d</sup>	29.2±2.6	4.4±1.5	3.46–1.48 <sup>d</sup>
2022.0±0.7	28.9±3.1	4.5±0.9	2.24–0.22
2192.8±0.6	25.6±2.6	4.0±0.8	2.24–0.050
2243.5±0.6	86.0±5.0	13.3±2.3	2.24–0
3537.7±1.2	7.8±1.6	1.2±0.3	3.76–0.22
3710.0±2.0	4.0±2.3	0.6±0.4	3.76–0.050
3761.1±2.0	5.7±2.1	0.9±0.4	3.76–0

<sup>a</sup>In  $^{31}\text{Mg}$  unless otherwise specified.

<sup>b</sup>Present in the decay scheme of  $^{29}\text{Na}$  [30], produced here in the  $2n$  channel, but its intensity could not be reliably appraised because of the close neighborhood of the strong 50.5 keV line.

<sup>c</sup>In  $^{29}\text{Mg}$  subsequent to  $\beta$ -delayed two-neutron emission offering an observable strength.

<sup>d</sup>In  $^{30}\text{Mg}$  subsequent to  $\beta$ -delayed one-neutron emission.

<sup>e</sup>Adopted value from Ref. [20] because of the presence in our spectrum of a contaminating line at this energy.

TABLE II. Gamma-ray branching ratios in  $^{31}\text{Mg}$ .

$E_i$ (keV)	$E_f$ (keV)	Gamma branching ratio
50	0	100
221	0	29±2
	50	71±2
673	0	28±2
	50	64±3
	221	8±2
945	50	100
1029	221	100
2243	0	58±2
	50	17±2
	221	19±2
	1029	6±1
3760	0	33±10
	50	23±11
	221	44±10
3814	2243	100

The energy and intensity of the  $\gamma$  rays observed in the  $\beta$  decay of  $^{31}\text{Na}$  are listed in Table I. The  $\gamma$  branching ratios in  $^{31}\text{Mg}$  are given in Table II. It is noteworthy that two weak  $\gamma$  rays arising in the deexcitation of  $^{29}\text{Mg}$  are observed. Only an upper limit on their intensity was given previously. Their actual detection is a definite argument in favor of a nonvanishing value of the  $\beta$ -delayed two-neutron probability in the  $\beta$  decay of  $^{31}\text{Na}$ .

### 1. Level scheme of $^{31}\text{Mg}$ resulting from the 0-n process

The disintegration scheme of  $^{31}\text{Na}$  ( $J^\pi = \frac{3}{2}^+$  [27,8]) is shown in Fig. 1. In comparison with the results of Ref. [20] and on the basis of our coincidence data, one level at 895 keV is invalidated. On the other hand, four previously unreported states are added to the excitation scheme of the final nucleus (see Table III).

The  $\beta$  intensity to the ground state of  $^{31}\text{Mg}$  is calculated assuming the  $P_n$  values of Ref. [28] and the absolute  $\gamma$  intensities as determined according to our decay scheme. Since several parameters affected by uncertainties occur in series in this calculation, the final value is not very precise. Nevertheless, our result (see Table III) is compara-

TABLE III. Beta intensities and  $\log ft$  values in the  $^{31}\text{Na}$   $\beta$  decay to bound levels in  $^{31}\text{Mg}$ .

$E_x$ (keV)	$I_\beta$ (per 100 decays)	$\log ft$
0	26±9	4.9
50.5±0.7	4.8±3.2	5.6
221.0±0.4	< 2.2	> 6.0
673.1±1.2	5.3±1.6	5.5
945.1±1.0	0.9±0.3	6.2
1028.6±0.8	< 1.1	> 6.1
2243.5±0.4	19.7±5.9	4.7
3759.9±1.0	2.6±0.9	5.3
3814.5±1.3	2.5±0.8	5.3

TABLE IV. Energy and intensity of  $\gamma$  rays observed in the  $\beta$  decay of  $^{31}\text{Na}$  and related to the  $\beta$ -delayed 1n channel.

$E_\gamma$ (keV)	$I_\gamma$ (relative)	$I_\gamma$ (per 100 decays)
305.6±0.3	13.6±1.3	2.0±0.7
985.1±0.4	12.0±2.2 <sup>a</sup>	1.8±0.7
1482.0±0.3	100	15.0±5.0
1820.2±0.6	20.0±2.2 <sup>a</sup>	3.0±1.0
1978.0±0.6	29.2±2.6	4.4±1.5

<sup>a</sup>Values taken from Ref. [20] because of a contamination in our spectrum.

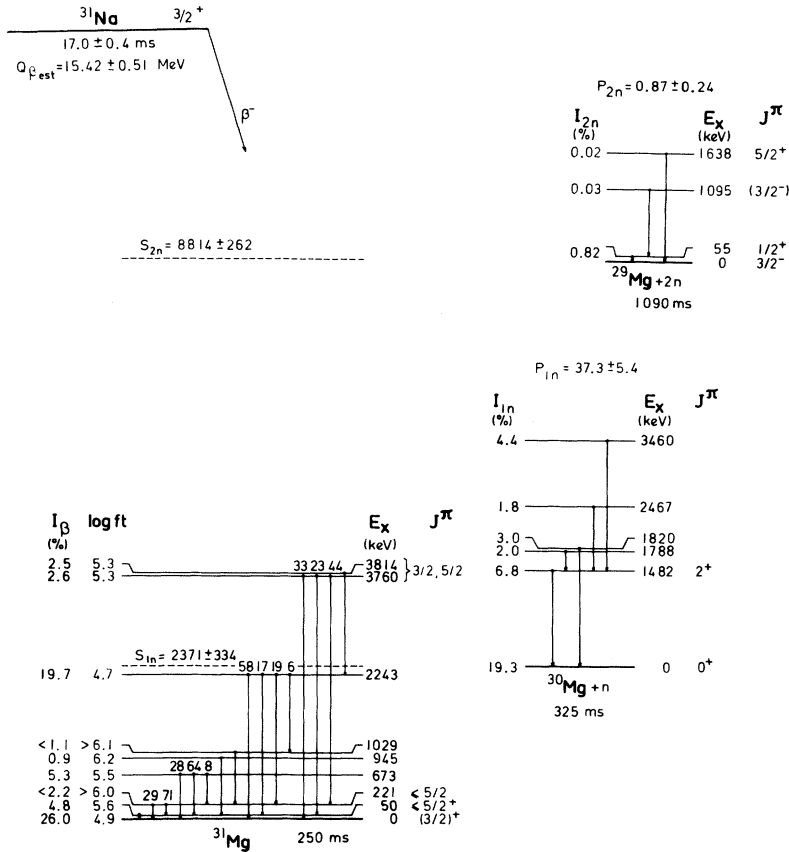
ble with the one given in Ref. [20], although somewhat smaller, which leads, but not sufficiently, to a more satisfactory agreement with theory as will be seen in Sec. IV.

Care was taken in this work to get reliable efficiency curves of the germanium detectors, even at low energy. An estimate of the  $\gamma$ -intensity balance of the first excited state at 50 keV, and consequently of its  $\beta$  feeding, can then be given. As a result, it was possible to bring into relief the strong difference between the  $\beta_0$  and the  $\beta_1$  branch intensities.

The 50 keV level was found to be relatively long lived. The measurement of its half-life was carried out by means of the observation of coincidences between fast signals corresponding to the  $\beta$  detection in a  $3\pi$  plastic scintillator surrounding the  $^{31}\text{Na}$  sources and  $\gamma$  detection in a  $\text{BaF}_2$  crystal (36 mm in diameter, 6 mm thick) viewed by a XP 2020 Q phototube. This latter device is known to exhibit excellent timing properties along with a sufficiently good resolution power at low energy, typically 20 keV full width at half maximum (FWHM) at 60 keV as measured with a  $^{241}\text{Am}$  standard. The biparametric spectrum obtained by storing the energy signals versus the time to amplitude converter response between the two detectors is shown in Fig. 2. The only delayed events correspond to the deexcitation of the 50 keV level. A conventional representation of its decay is displayed in the inset. The deduced half-life  $T_{1/2}$  is equal to  $16.0 \pm 2.8$  ns.

The  $\beta$  intensity to the second excited state at 221 keV appears now to be very low. Only an upper limit of 2.2% can be inferred from the  $\gamma$  imbalance, in contrast with Ref. [20], where an actual branch of 5.4% was assumed. The corresponding  $\log ft$  value differs by at least one unit.

We establish a new level at 673 keV, substantially populated according to our results. The evidence for the 673 keV  $\gamma$  ray to deexcite a level of the same energy toward the ground state in competition with the 623 keV  $\gamma$  ray going to the first excited 50 keV state discussed above was not considered previously, as a 623 keV line occurs alike as a transition in the descendent  $^{31}\text{Al}$   $\beta$  decay (2316.8–1695.0 keV in  $^{31}\text{Si}$ ). The existence of a doublet is necessary to explain the whole observed intensity of the 623 keV line. This assignment is supported by the  $\gamma$ - $\gamma$  measurements: Figure 3 shows clearly a 623 keV line in coincidence with a 50 keV one. A further and conclusive argument is the presence of a 452 keV line coincident

FIG. 1. Disintegration scheme of  $^{31}\text{Na}$ .

with the 50, 171, and 221 keV lines as displayed in Fig. 4. This ray corresponds to an additional decay mode of the 673 keV level. It is not easily detectable in the direct spectrum, being located close to the right edge of a strong line at 444 keV due to the descendent (688.1–244.3 keV in  $^{30}\text{Al}$ ).

Figure 3 illustrates another new result. It clearly appears there that the 895 keV line originating in the deexcitation of  $^{31}\text{Na}$  should not be attributed to a transition to the ground state but to the first excited state at 50 keV, which is a firm signature for a new level at 945 keV.

Going on upwards, the levels at 1029 and 2243 keV are confirmed. In the case of the  $\beta$  branch intensity to the first one, we are only able to secure an upper limit, which is not in contradiction, however, with the known results.

Finally, we locate two new levels at 3760 and 3814 keV on the basis of  $\gamma$ - $\gamma$  measurements. Strong electromagnetic deexcitation modes of states situated above the neutron separation energy were already encountered in previous works, in this mass region, in particular in  $^{48,49}\text{K}$   $\beta$ -decay studies [29].

## 2. $\beta$ -delayed neutron emissions from $^{31}\text{Na}$

The energies and intensities of  $\gamma$  rays observed in the  $\beta$ - $1n$  channel are reported in Table IV. The absolute intensities of the neutron feeding of six levels in  $^{30}\text{Mg}$  including the ground state are listed in Table V. Normalization is obtained via  $\gamma$ -ray intensities compared to those noticed in the  $^{31}\text{Na}$  ( $\beta$ )  $^{31}\text{Mg}$  process. The total of the

neutron branches toward the ground state is taken as the difference between the  $P_n$  value [28] and the normalized strength populating the excited levels. No additional states, in comparison with those reported [20], are observed.

In a similar way, we inferred the corresponding quantities for the  $2n$  process. The detection of two  $\gamma$  rays at 1040 and 1638 keV gives evidence of a weak neutron strength to levels at 1095 and 1638 keV in  $^{29}\text{Mg}$  (Table I

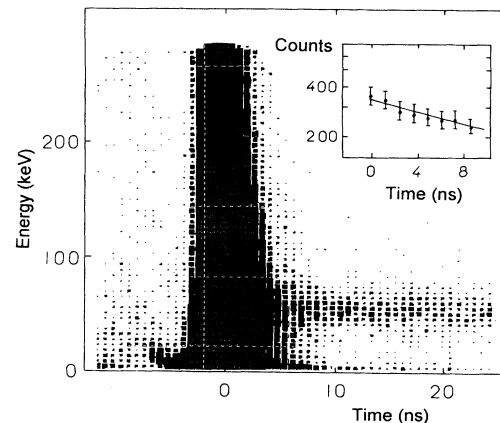


FIG. 2. Delayed coincidences taken in the decay of  $^{31}\text{Na}$  with the NE102 plastic  $\beta$  detector and a small  $\text{BaF}_2$  scintillator. In the inset the decay curve of the 50 keV gate, a least-squares fit leads to the value of  $T_{1/2} = 16.0 \pm 2.8$  ns.

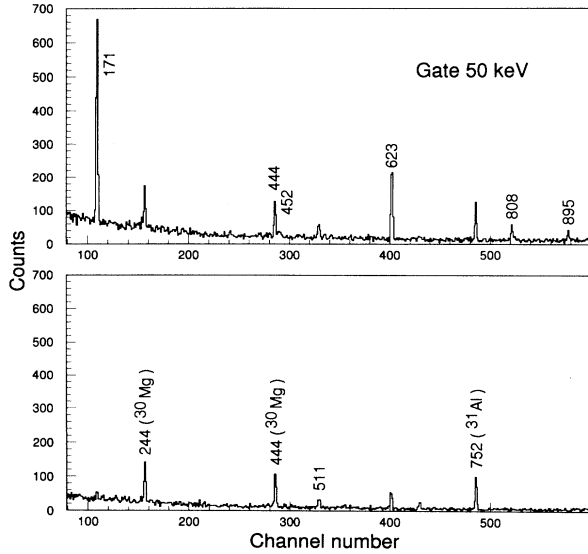


FIG. 3. Partial view of the 50 keV ray gated spectrum showing the substantial enhancement of the 623 keV line superposed on the longer-lived component due to the descendant, the prominent 171 keV peak, a weak line at 452 keV, and two rays at 808 and 895 keV. The lower part of the figure is the corresponding background.

and Fig. 5). The existence of the 55 keV line is known from a previous work [30]. It cannot be observed in the present work, being masked by the strong deexcitation peak of the first level in  $^{31}\text{Mg}$  at almost the same energy. Therefore it was not possible to estimate the amount of neutron strength, implying separately each member of the  $^{29}\text{Mg}$  ground-state doublet.

### B. Experimental $\beta$ decay of $^{31}\text{Mg}$

As in the case of  $^{31}\text{Na}$ , the half-life of  $250 \pm 30$  ms and the  $P_{1n}$  value were taken from Ref. [28]. A new estimate for the  $Q_\beta$  value was computed with the help of data published in Refs. [16,17,26]. Yet again the obtained result of  $11.69 \pm 0.27$  MeV is not significantly different from 11.42 MeV adopted previously. The neutron separation energy  $S_n$  originates from the same sources.

The  $\gamma$  rays attributed to transitions in the  $^{31}\text{Al}$  nucleus are listed in Table VI along with their intensity and as-

TABLE V. Intensity of neutron branches populating excited states in  $^{30}\text{Mg}$ .

$E_x(^{30}\text{Mg})$ (keV)	$I_n$ (per 100 decays)
0	$19.3 \pm 5.7^a$
1482	$6.8 \pm 1.4$
1788	$2.0 \pm 0.3$
1820	$3.0 \pm 0.5$
2467	$1.8 \pm 0.4$
3460	$4.4 \pm 0.7$

<sup>a</sup>Deduced from the  $P_n$  value ( $37.3 \pm 5.4\%$ ) and from the absolute neutron branch intensity to excited levels ( $18.0 \pm 1.7\%$ ).

TABLE VI. Energy and intensity of  $\gamma$  rays observed in the  $\beta$  decay of  $^{31}\text{Mg}$ .

$E_\gamma$ (keV)	$I_\gamma$ (relative)	$I_\gamma$ (per 100 decays)	Transition (MeV)
$666.2 \pm 0.7$	$34.0 \pm 1.8$	$13.4 \pm 2.3$	1.61–0.95
$904.0 \pm 0.8$	$5.3 \pm 0.6$	$2.1 \pm 0.4$	4.14–3.24
$946.6 \pm 0.5$	$78.3 \pm 4.0$	$30.8 \pm 5.2$	0.95–0
$1612.8 \pm 0.4$	$100(\pm 5.1)$	$39.4 \pm 6.6$	1.61–0
$1626.2 \pm 0.5$	$63.6 \pm 3.3$	$25.1 \pm 4.2$	3.24–1.61
$1820.0 \pm 0.8$	$8.8 \pm 1.2$	$3.5 \pm 0.7$	3.43–1.61
$2487.6 \pm 1.5$	$4.8 \pm 0.8$	$1.9 \pm 0.4$	3.43–0.95
$2529.8 \pm 1.0$	$8.7 \pm 0.8$	$3.4 \pm 0.6$	4.14–1.61
$2676.1 \pm 1.0$	$7.7 \pm 0.8$	$3.0 \pm 0.6$	3.62–0.95
$2949.0 \pm 1.0$	$12.3 \pm 1.1$	$4.8 \pm 0.9$	4.56–1.61
$3196.2 \pm 1.0$	$13.0 \pm 1.3$	$5.1 \pm 1.0$	4.14–0.95
$3431.8 \pm 1.2$	$16.2 \pm 1.3$	$6.4 \pm 1.1$	3.43–0
$3621.9 \pm 1.3$	$18.2 \pm 1.3$	$7.2 \pm 1.3$	3.62–0
$4201.1 \pm 1.4$	$5.7 \pm 0.9$	$2.2 \pm 0.5$	5.15–0.95
$4809.0 \pm 1.5$	$2.3 \pm 0.6$	$0.9 \pm 0.3$	4.81–0

signment. They are similar to those of Ref. [20]; however, the assignment of all lines could now be established.

In Table VII are shown the  $\gamma$  branching ratios as inferred from our measurement. Table VIII gives the  $\beta$  branching and the corresponding  $\log ft$  values.

The level scheme of  $^{31}\text{Al}$  established in this work and displayed in Fig. 6 contains several new results important for the description of the low-energy structure of  $^{31}\text{Al}$ . The most interesting one is the suppression of a state at 2530 keV, assumed to arise from the decay of a 3434 keV level through a 904 keV line [20]. It is easy to rule out this assertion on account of our coincidence data (Figs. 7 and 8). The two lines (904 and 2530 keV) are well interpreted if one considers the existence of a new state at 4143 keV, which they deexcite. According to observed coincidences, this state is in addition connected with the 3196 keV line formerly assumed to be emitted from the 4809 keV level. An additional argument in this sense is

TABLE VII. Gamma-ray branching ratios in  $^{31}\text{Al}$ .

$E_i$ (keV)	$E_f$ (keV)	Gamma branching ratio
947	0	100
1613	0	$75 \pm 2$
	947	$25 \pm 2$
3239	1613	100
3434	0	$54 \pm 1$
	947	$16 \pm 1$
	1613	$30 \pm 1$
3622	0	$70 \pm 1$
	947	$30 \pm 1$
4143	947	$48 \pm 1$
	1613	$32 \pm 1$
	3239	$20 \pm 1$
4562	1613	100
4809	0	100
5148	947	100

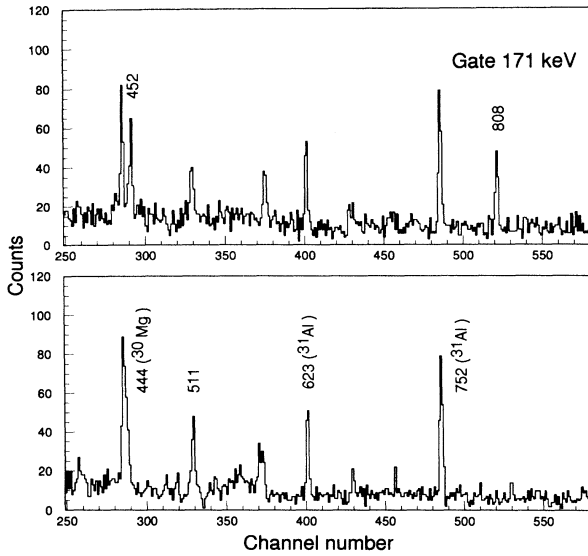


FIG. 4. Partial view of the 171 keV gate showing the presence of the 452 keV line along with the 808 keV one. In the lower part corresponding to the background, the contaminating lines are labeled by the parent isotope.

shown in Fig. 8, where a strong lack for the 666 keV (1613–947 keV) line intensity is observed compared to the 947 keV one.

At higher energy, we locate a new state at 4562 keV, revealed by 2949–666–947 coincidences. Finally, another new level, involving 4201–947 coincidences, is placed at

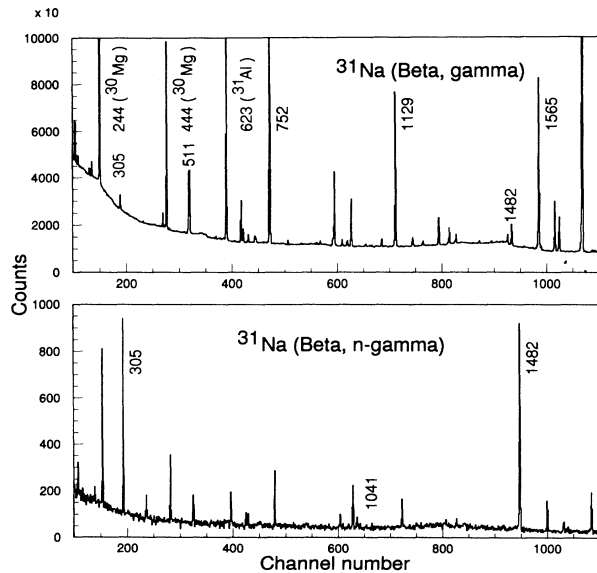


FIG. 5. Partial  $\gamma$  spectrum of the  $^{31}\text{Na}$  ( $\beta, \gamma$ ) decay is shown in the top part of the figure and compared in the same energy range to the spectrum taken in coincidence with neutrons in the bottom part. Note the enhancement of the  $\gamma$  lines subsequent to the  $1n$  process; lines arising in the  $2n$  process (e.g., 1041 keV) are not substantially favored by the coincidence technique, probably because of the energy threshold in the neutron detection chain.

TABLE VIII. Beta intensities and  $\log ft$  values in the  $^{31}\text{Mg}$   $\beta$  decay to bound levels in  $^{31}\text{Al}$ .

$E_x$ (keV)	$I_\beta$ (per 100 decays)	$\log ft$
0	$12.9 \pm 6.0$	5.8
947	$5.2 \pm 2.1$	6.0
1613	$16.1 \pm 3.7$	5.3
3239	$23.1 \pm 4.0$	4.9
3434	$11.7 \pm 2.1$	5.1
3622	$10.3 \pm 1.8$	5.1
4143	$10.7 \pm 1.8$	5.0
4562	$4.9 \pm 0.9$	5.1
4809	$0.9 \pm 0.2$	5.8
5148	$2.3 \pm 0.5$	5.4

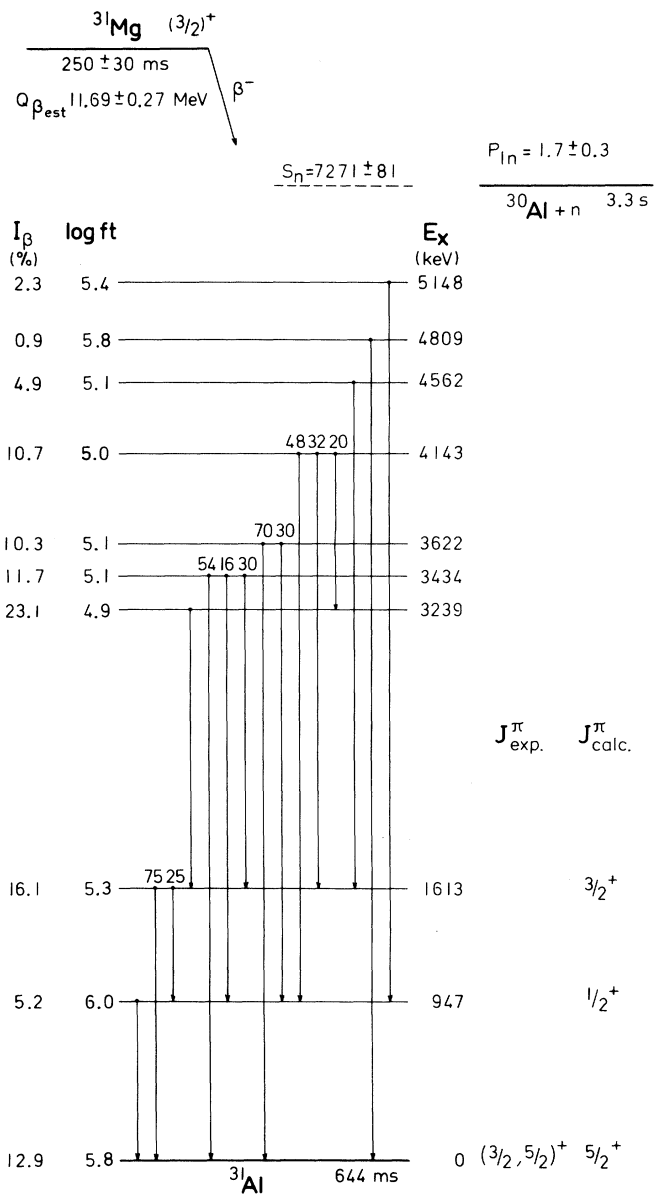


FIG. 6. Disintegration scheme of  $^{31}\text{Mg}$ . The column at the right gives the theoretical  $J^\pi$  values from Ref. [32].

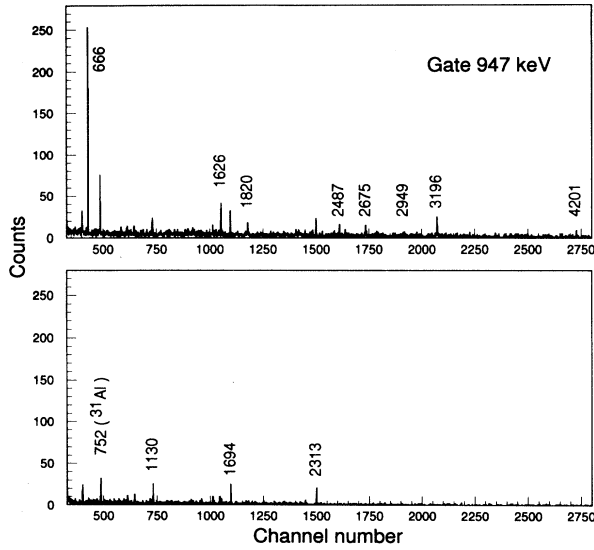


FIG. 7. Gate on the 947 keV line corresponding to the deexcitation of the first level in  $^{31}\text{Al}$ . The lower part of the figure shows the corresponding background. These results support the whole framework of the proposed  $^{31}\text{Mg}$  decay scheme.

5148 keV.

As no appreciable  $\gamma$  strength in  $^{31}\text{Al}$  remains now unexplained, we can deduce the  $\beta_0$ -intensity value of  $12.9 \pm 6.0$  from the absolute  $\gamma$  intensities. Because of the faintness of the  $\beta$ -delayed neutron channel ( $P_n = 1.7 \pm 0.3$  [28]), no reasonable possibility of observing  $\gamma$  lines from  $^{30}\text{Al}$  is expected.

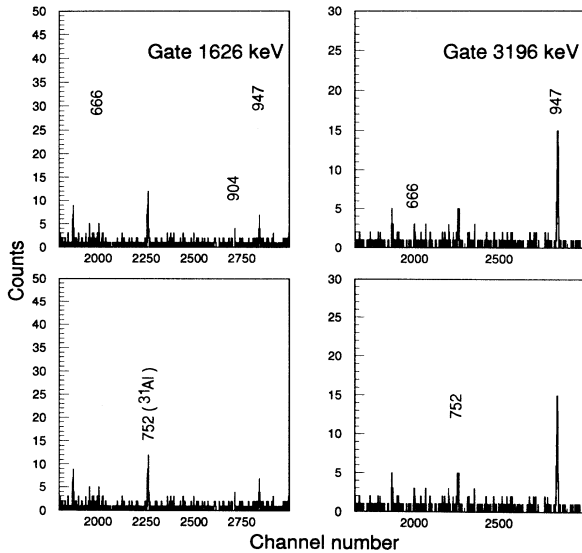


FIG. 8. Upper left: gate on the 1626 keV line emphasizing the components of the  $4143 \rightarrow 3239 \rightarrow 947 \rightarrow 0$  cascade (background below). Upper right: gate on the 3196 keV line showing the outstanding presence of the 947 keV transition, whereas the 666 keV peak does not exhibit the expected strength if the 3196 keV ray assignment of Ref. [20] is assumed. However, a weak contribution of this process cannot be excluded.

### C. Experimental $\beta$ decay of $^{32}\text{Na}$

The  $\beta$  decay of  $^{32}\text{Na}$  was studied with the same techniques as in the case of mass 31. However, the experimental conditions were less favorable on account of the following points: (i) a weaker production yield ( $\leq 15$  atoms/s) due to the increased remoteness from stability; (ii) the disturbing presence of  $^{32}\text{Al}$  directly produced but not separated from the isobar  $^{32}\text{Na}$  by the mass spectrometer, competing with the part arising in the radioactive fission; and (iii) a cumbersome background resulting from the  $A = 128$  chain corresponding to multicharged ions (mainly  $^{128}\text{In}$  and its descendants,  $A = 4 \times 32$ ,  $q = 4^+$ ), neither eliminated by the separator.

The  $\gamma$ -ray energies and intensities observed in and attributed to the decay of  $^{32}\text{Na}$  are listed in Table IX. In our experiment, no attempt was made to yield high precision on  $\gamma$ -ray energy values since during the early stage of analysis a fair agreement with the published values was noted. The intensity of peaks perturbed by contaminating lines is taken from Ref. [20]. The present value for the 1973 keV line is estimated from coincidence data. In the single spectra, it is completely overwhelmed by a strong line of the same energy arising in the  $^{128}\text{In}$  decay. The proposed decay scheme of  $^{32}\text{Na}$  is shown in Fig. 9. Half-life values are taken from Ref. [28]. Neutron separation energies are inferred from mass systematics [26]. The  $^{32}\text{Na}$   $Q_\beta$  value is revised in comparison [28], taking into account the recent mass excess measurements of Refs. [18,19] for  $^{32}\text{Mg}$ .

The disintegration of  $^{32}\text{Na}$  splits up into three channels

TABLE IX. Energy and intensity of  $\gamma$  rays observed in the  $\beta$  decay of  $^{32}\text{Na}$ .

$E_\gamma^a$ (keV)	$I_\gamma$ (relative)	$I_\gamma$ (per 100 decays)	Transition <sup>a</sup> (MeV)
50 <sup>b,c</sup>			0.05–0 <sup>c</sup>
171 <sup>c</sup>	21.9±3.5	13.3±2.5	0.22–0.05 <sup>c</sup>
221 <sup>c</sup>	8.9±1.8	5.4±1.3	0.22–0 <sup>c</sup>
240 <sup>c</sup>	9.7±1.1	5.9±1.0	0.46–0.22 <sup>c</sup>
694	3.8±1.6 <sup>d</sup>	2.2±1.3	
885	100	58.8±7.9	0.88–0
895 <sup>e</sup>	5.1±2.6	3.1±1.6	0.94–0.05 <sup>c</sup>
929 <sup>e</sup>	4.0±1.9	2.4±1.2	1.39–0.46 <sup>c</sup>
1232	4.8±1.7	2.8±1.0	2.12–0.88
1436	9.8±2.5	5.8±1.6	2.32–0.88
1482 <sup>e</sup>	4.9±2.2	3.0±1.4	1.48–0 <sup>e</sup>
1783	8.3±2.0 <sup>d</sup>	4.9±1.3	4.82–3.04
1973	19.7±2.5	11.6±2.5	2.86–0.88
2152	48.5±3.7	28.5±4.1	3.04–0.88
2551	10.2±2.5	6.0±1.6	2.55–0
3935	18.3±3.7	10.8±2.6	4.82–0.88

<sup>a</sup>In  $^{32}\text{Mg}$  unless otherwise specified.

<sup>b</sup>Known to occur in the  $^{31}\text{Mg}$  deexcitation, but its intensity could not be reliably determined because of the closeness of the experimental threshold.

<sup>c</sup>Subsequent to  $\beta$ -delayed one-neutron emission.

<sup>d</sup>Adopted value from Ref. [20] because of the presence in our spectrum of a contaminating line at this energy.

<sup>e</sup>Subsequent to  $\beta$ -delayed two-neutron emission.

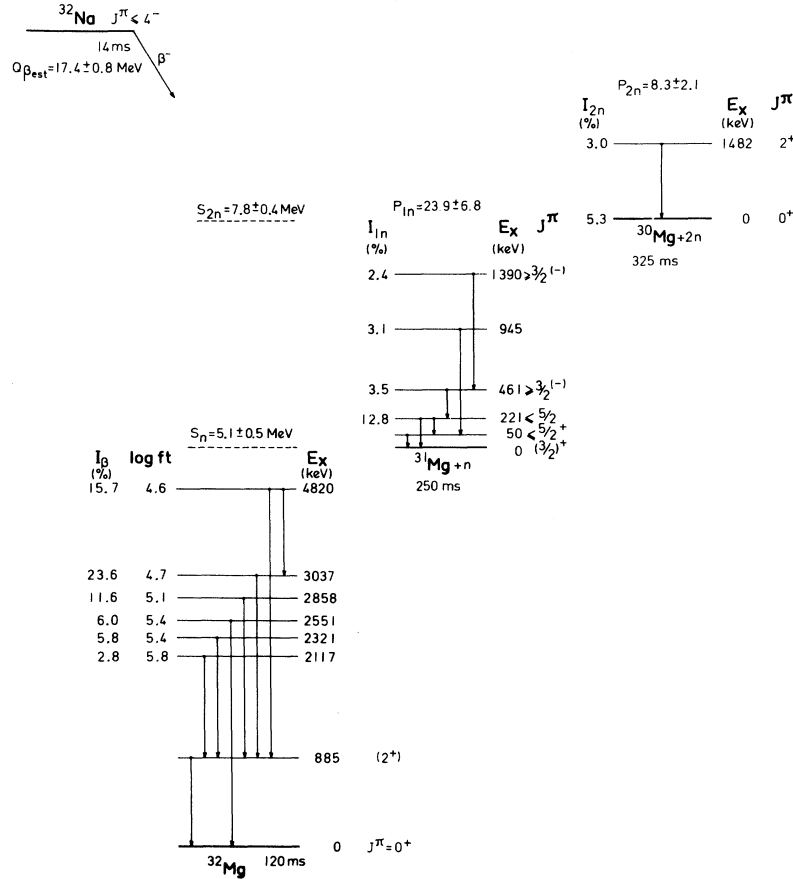


FIG. 9. Decay scheme for  $^{32}\text{Na} \rightarrow ^{32}\text{Mg}$  and the competing neutron emission.

where the  $P_{1n}$  and  $P_{2n}$  probabilities quoted in Ref. [20] are carried. From crude shell model considerations, the  $^{32}\text{Na}$  ( $Z=11$ ,  $N=21$ ) ground state has negative parity. Hence allowed  $\beta$  transitions can feed only negative parity states (bound or unbound) in  $^{32}\text{Mg}$ .

The knowledge of the pure ( $\beta, \gamma$ ) process, to the exclusion of beta-delayed neutron channels, feeding levels in  $^{32}\text{Mg}$ , the most deformed nucleus known in the mass region, gains some substance in comparison with the previous scheme. Three additional states are located at low energy (2117, 2321, and 2551 keV) on the basis of  $\gamma$ - $\gamma$  coincidences involving the first excited level for the two former ones (Fig. 10). As for the latter at 2.55 MeV, the nonobservation of any coincidence relation leads us to conclude in favor of a ground-state deexcitation of this level. So three out of four  $\gamma$  rays emitted by the  $^{32}\text{Mg}$  nucleus, unexplained prior to this work, are assigned. The only noninterpreted one lies at 694 keV, which seems too low to correspond to a level at this energy; on the other hand, no indication is obtained on a hypothetical cascading process, implying another known level. Nevertheless, according to Table IX, this lack amounts to an almost negligible part of the whole  $\gamma$  strength. Absolute beta intensities deduced from gamma imbalances are given in Table X along with the corresponding  $\log ft$  values. We note that all the observed  $\beta$  transitions have an allowed character and hence populate negative parity states in

$^{32}\text{Mg}$ . No perceptible direct  $\beta$  feeding of the ground and 885 keV states can take place since they are of positive parity. The absolute arithmetic  $\gamma$  imbalance of the 885 keV level is equal to  $-0.7 \pm 9.8$ , which is compatible with a vanishing value.

The knowledge of the beta-delayed one-neutron channel is improved alike. A 240 keV  $\gamma$  ray previously attributed to  $^{32}\text{Mg}$  [20], but not placed in the scheme, is clearly detected in coincidence with neutrons and with the deexciting rays of the two first states of  $^{31}\text{Mg}$  (Figs. 11 and 12). So it appears to be emitted in all probability by a state located at 461 keV. It is additionally in coin-

TABLE X. Beta branch intensities and corresponding  $\log ft$  values in the partial decay scheme of  $^{32}\text{Na}$  to  $^{32}\text{Mg}$  levels.

$E_x$ (keV)	$I_\beta$ (per 100 decays)	$\log ft$
0		
885		
2117	$2.8 \pm 1.0$	5.8
2321	$5.8 \pm 1.6$	5.4
2551	$6.0 \pm 1.6$	5.4
2858	$11.6 \pm 2.5$	5.1
3037	$23.6 \pm 4.3$	4.7
4820	$15.7 \pm 2.9$	4.6

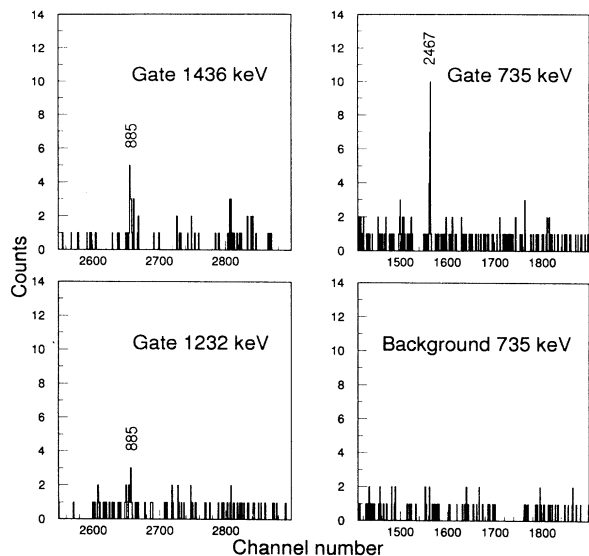


FIG. 10. Upper left and bottom left: gates on the 1436 and 1232 keV lines revealing the population of the first excited state of  $^{32}\text{Mg}$  (background has been subtracted). The right part shows the evidence for a cascade in the  $^{32}\text{Mg} \rightarrow ^{32}\text{Al}$  decay.

cidence with a weak 929 keV  $\gamma$  ray not listed until now, which contributes to the feeding of a 461 keV level from a new state situated at 1390 keV.

A severe discrepancy between the intensity of the 240 keV ray given in Ref. [20] ( $I_{\text{abs}} = 16.6 \pm 3.2$ ) and in the present work ( $I_{\text{abs}} = 5.9 \pm 1.0$ ) remains unexplained, the

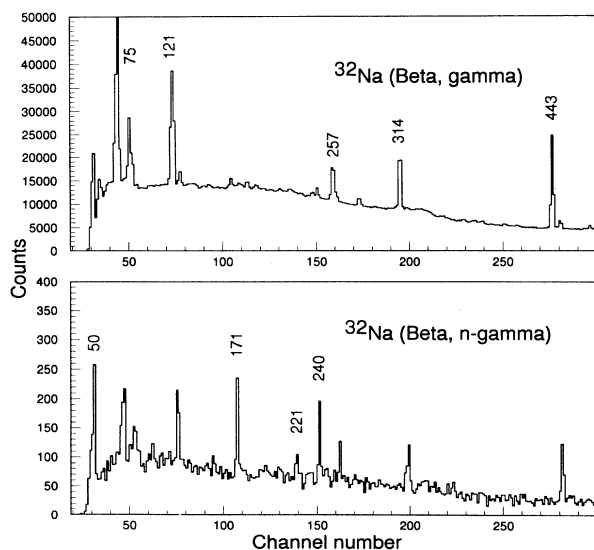


FIG. 11. Comparison of the direct  $\gamma$  spectrum of the  $^{32}\text{Na}$  ( $\beta, \gamma$ ) process to the  $\gamma$  spectrum taken in coincidence with neutrons. The enhancement of the lines at 171, 221, 240, and 929 keV (not shown) provides a clear evidence for the population of a set of levels in  $^{31}\text{Mg}$  distinct from those populated in the  $^{31}\text{Na}$  decay.

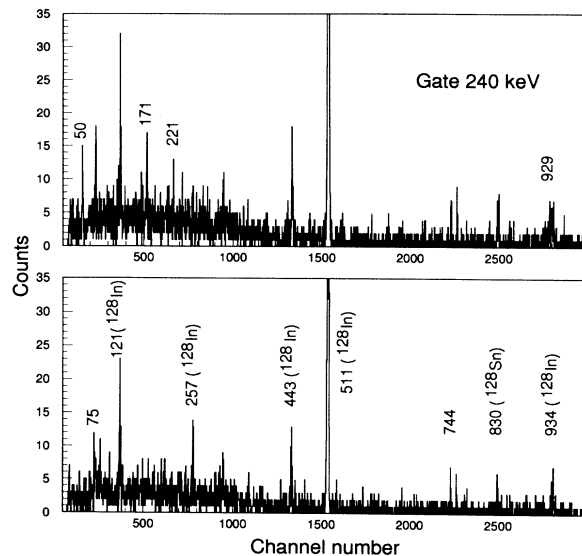


FIG. 12. Gate on the 240 keV peak, in the  $\gamma$ - $\gamma$  coincidences, from the  $^{32}\text{Na}$  decay, establishes the cascade relations of the set of levels revealed by the  $n, \gamma$  coincidences (background in the lower part of the figure).

former one being basically inconsistent with the new scheme. One also should note the enhanced intensities, nearly by a factor 2, of the lines deexciting the 221 keV level. A quantitative measurement of the 50 keV  $\gamma$  ray could not be undertaken because of its closeness to the detection threshold. Nevertheless, its existence is clearly observed.

In neutron emissions the lowest multipole order is favored (usually  $l=0$ ), and so delayed neutrons most likely feed negative parity states in  $^{31}\text{Mg}$ . So the observed  $\gamma$  cascade should imply three negative parity levels: 1390 keV ( $\pi = -$ )  $\rightarrow$  461 keV ( $\pi = -$ )  $\rightarrow$  221 keV ( $\pi = -$ )  $\rightarrow$  50 keV ( $\pi = +$ ). Clearly, such states could not be populated in the  $^{31}\text{Na}$  ( $J^\pi = \frac{3}{2}^+$ )  $\beta^- \gamma$  process. The theoretical part of this paper (see Sec. IV) discloses the intruder character of the negative parity states.

The neutron branching ratios for the  $\beta$ -delayed one- and two-neutron emissions are listed in Table XI. Be-

TABLE XI. Neutron branching ratios in the one- and two-neutron  $\beta$ -delayed channels of the  $^{32}\text{Na}$  decay scheme.

One-neutron channel		Two-neutron channel	
$E_x$ (keV)	$I_n$ (per 100 decays)	$E_x$ (keV)	$I_n$ (per 100 decays)
0		0	$5.3 \pm 2.5^a$
50		1482	$3.0 \pm 1.4$
221	$12.8 \pm 3.0$		
461	$3.5 \pm 1.6$		
945	$3.1 \pm 1.6$		
1390	$2.4 \pm 1.2$		

<sup>a</sup>Deduced from the  $P_{2n}$  value [28] and the absolute  $\gamma$  strength emitted by  $^{30}\text{Mg}$ .

cause of their positive parity, the ground and first excited states of  $^{31}\text{Mg}$  are not expected to be substantially fed by neutron branches.

In the delayed  $2n$  branch, an overall parity change is observed from  $^{32}\text{Na}$  ( $\pi = -$ ) to the ground and  $2^+$  states of  $^{30}\text{Mg}$ . This seems difficult to interpret with a dineutron ( $S=0$ ) emission, while it could be quite normal in sequential emission with different  $l$  values ( $l=0$  and  $1$ ).

#### D. $\beta$ decay of $^{32}\text{Mg}$

Literature data [20] on this process are very scarce. The three previously reported lines (735, 2467, and 2765 keV) are confirmed in our direct spectrum. Valuable information has been obtained in our  $\gamma$ - $\gamma$  experiment where a coincidence relationship between the 735 and 2467 keV  $\gamma$  rays is observed as shown in Fig. 10. The weaker intensity of the latter one, in agreement with results quoted in Ref. [20], means that a 735 keV level could be the intermediate state of the  $\gamma$  cascade (3202 keV  $\rightarrow$  735 keV  $\rightarrow$  0).

#### E. Extraction of some spin-parity assignments

A detailed comparison of the experimental level structure of  $^{31}\text{Al}$  populated either by  $\beta$  decay or by heavy-ion transfer reactions, to  $sd$ -shell model calculations, has been discussed by Woods *et al.* [21]. The new data confirm the agreement for the energies and  $\gamma$  transitions of the first three states, whose theoretical spin and energy values are  $\frac{5}{2}^+$  (g.s.),  $\frac{1}{2}^+$  (944 keV), and  $\frac{3}{2}^+$  (1744 keV). The suppression of the 2530 keV experimental level improves the analogy at higher energies, but the electromagnetic properties are poorly reproduced by these calculations.

##### 1. States in $^{31}\text{Mg}$

The observed allowed character of  $\beta_0$  and  $\beta_2$  transitions in the  $^{31}\text{Mg} \rightarrow ^{31}\text{Al}$   $\beta$  decay gives strong support to a limitation  $J^\pi = (\frac{3}{2}, \frac{5}{2})^+$  of the spin and parity values of the  $^{31}\text{Mg}$  g.s. The  $\frac{5}{2}^+$  assignment is ruled out by the  $\log f_1 t$  (8.4) of the  $\beta_1$  transition if  $J^\pi = \frac{1}{2}^+$  is assumed for the 947 keV state; a second-forbidden nonunique transition would amount, at most, to a  $1.5 \times 10^{-4}$   $\beta$  branch.

In the comparison made in Ref. [21], the experimental  $\beta_0$  intensity shows a severe reduction, which will be discussed in Sec. IV. The  $^{31}\text{Na}$  ( $J = \frac{3}{2}$ )  $\rightarrow$   $^{31}\text{Mg}$  allowed  $\beta_0$  transition introduces similarly a limitation for the spin value of the  $^{31}\text{Mg}$  g.s.,  $J = (\frac{1}{2}, \frac{3}{2}, \frac{5}{2})$ , the values  $\frac{1}{2}$  and  $\frac{3}{2}$  being rejected above.

The measured half-life (Sec. III A 1) of the first excited state in  $^{31}\text{Mg}$  limits the multipole order of the 50 keV transition to a dipole. The corresponding retardation factors are  $\Gamma/\Gamma_w = (3.4 \pm 0.6) \times 10^{-4}$  Weisskopf units (W.u.) for  $E1$  and  $(1.1 \pm 0.2) \times 10^{-2}$  W.u. for  $M1$  transitions. The nonobservation of the measurable half-life for higher levels (Fig. 2) limits the multipolarity of the 221 and 171 keV transitions to  $L=1$ . An  $L=2$  multipolarity is excluded for the two transitions as it would correspond to an unlikely value for the  $E2$  transition strength ( $> 40$

W.u. for the 221 keV transition). The limit of the multipolarity sets a restriction to the spin of the 221 keV state. These limits are reported in Fig. 1 using also the results of the theoretical discussion (Sec. IV).

Among the excited state of  $^{31}\text{Mg}$  populated from  $^{31}\text{Na}$  via allowed  $\beta$  transitions, the two unbound levels at 3760 and 3814 keV ( $J^\pi = \frac{1}{2}^+, \frac{5}{2}^+$ ) are observed to decay by  $\gamma$  emission. The  $J^\pi = \frac{1}{2}^+$  value can be eliminated for these two levels as it would give rise to  $l=0$  neutron emission dominating the process.

The five excited states of  $^{30}\text{Mg}$  populated in the  $^{31}\text{Na}$  ( $J^\pi = \frac{3}{2}^+$ )  $\beta$ - $1n$  channel also have been observed previously in the  $^{30}\text{Na}$  ( $J^\pi = 2^+$ ) study [31]. This situation is a particular case which will not be encountered in the  $^{32}\text{Na}$  decay discussed below.

The  $^{31}\text{Na}$   $\beta$ - $2n$  process populates positive and negative parity states in  $^{29}\text{Mg}$ . This feature is similar to the one noted and discussed above for the  $^{32}\text{Na}$   $\beta$ - $2n$  decay.

##### 2. Consequences for the $^{32}\text{Na}$ ground state

An interesting finding of this work is a selective population of new states related by a  $\gamma$  cascade [ $E_x(^{31}\text{Mg})$ : 461 and 1390 keV] through the  $\beta$ - $1n$  decay of  $^{32}\text{Na}$ . The nonobservation of these levels in the  $^{31}\text{Na}$   $\beta$  decay suggests the presence of a set of levels in  $^{31}\text{Mg}$  either of negative parity or of high spin value. This latter assumption is incompatible with their low multipolarity  $\gamma$  decay. The difference of  $^{31}\text{Mg}$  states populated in the two processes may thus result form a different parity of the parent states:  $^{31}\text{Na}$  ( $J^\pi = \frac{3}{2}^+$ ),  $^{32}\text{Na}$  ( $\pi = -$ ). This interpretation is similar to the prediction of the parity of  $^{32}\text{Na}$  by a simple shell model corresponding to a  $0\hbar\omega(1fp)$  or  $2\hbar\omega(3fp)$  g.s. configuration. A negative parity of  $^{32}\text{Na}$  would also explain the absence of  $\beta_0$  and  $\beta_1$  branches in the  $^{32}\text{Na}$  decay. The discussion relative to the  $2^+$  assignment to the 885 keV level made in Ref. [20] is substantiated by our work. From the present experiment, seven excited  $^{32}\text{Mg}$  states are now reported in the  $^{32}\text{Na}$  decay. For all except one the deexcitation takes place through a  $\gamma$  cascade involving the 885 keV ( $2^+$ ) state. The 2551 keV level populated by an allowed  $\beta$  transition is observed to decay only to the ground state. This allows one to set an upper limit on the spin of the  $^{32}\text{Na}$  g.s.: From our  $\beta$ - $\gamma$  measurement, the 2.55 MeV state has a half-life lower than 100 ns, limiting the multipole order of the g.s.  $\gamma$  transition to a dipole, quadrupole, or  $E3$ . Hence the spin of this level is  $J \leq 3$ . The allowed character of the  $\beta$  feeding ( $\log ft = 5.4$ ) of this level imposes no parity change and limits the  $^{32}\text{Na}$  g.s. spin value to  $J \leq 4$ .

Among the known treatments of nuclei in this region, the calculation by Warburton *et al.* [10] considers different possible interpretations for the  $^{32}\text{Na}$  g.s., implying either negative parity [in the case of  $0\hbar\omega(1fp)$ ,  $J^\pi = 2^- - 6^-$  and  $2\hbar\omega(3fp)$ ,  $J^\pi = 0^-$  configurations] or positive parity with low spin value,  $J^\pi = 0^+$ , resulting from a coupling in a  $1\hbar\omega(2fp)$  configuration.

From this experiment it is difficult to assess a definite value to the ground state. Nevertheless, with our results obtained in the  $\beta$ - $1n$   $^{32}\text{Na}$  study, the  $1\hbar\omega(2fp)$ ,  $J^\pi = 0^+$ ,  $^{32}\text{Na}$  g.s. configuration is the less plausible as (a) the ob-

served population of several states cascading by  $\gamma$  decay to the  $^{31}\text{Mg}$  g.s. suggests a higher spin value for  $^{32}\text{Na}$ , and (b) the strong  $\beta$ - $n$  feeding of the  $\frac{3}{2}^+$   $^{31}\text{Mg}$  g.s. would be expected and is not observed.

#### IV. SHELL MODEL CALCULATION AND COMPARISON WITH EXPERIMENT

Many of the novel aspects of nuclear structure found near the  $N=20$  shell closure far from stability can be understood in a shell model context, provided the valence space includes the  $sd$  shell and the lowest orbits of the  $fp$  shell. We shall approach the decays of  $^{32}\text{Na}$ ,  $^{31}\text{Na}$ , and  $^{31}\text{Mg}$  using the same model, valence space, and interaction already applied to other nuclei of the region [8,9,11]. Among the conclusions of these references, one is of major importance here: The fact that the transition from normal  $sd$ -shell nuclei to a region of deformation is predicted to take place at  $N=19$ . Therefore nuclei such as  $^{32}\text{Na}$  ( $N=21$ ),  $^{31}\text{Na}$  ( $N=20$ ), and  $^{32}\text{Mg}$  ( $N=20$ ) would belong to the deformation region (sometimes called also inversion region or intruder region, because the nuclear wave functions of the ground states and of the excited states at low energy are dominated by  $2p$ - $2h$  configurations, i.e., intruder configurations), while nuclei with  $N=18$  would be fully normal and nuclei with  $N=19$  transitional.

In the  $A=31$  decays explored in this work, we find these three sorts of nuclei. Besides, in the  $A=32$  case the decay proceeds through the negative parity states of  $^{32}\text{Mg}$ , which are  $1p$ - $1h$  intruders. Therefore the comparisons between theory and experiment cover most possible situations.

##### A. Decay $^{31}\text{Na} \rightarrow ^{31}\text{Mg}$

In our calculation the ground state of  $^{31}\text{Na}$  is  $\frac{3}{2}^+$ , in agreement with the experimental result. It is fully (90%) dominated by configurations with two neutrons in the  $fp$  shell (intruders).

In order to have a good description of  $^{31}\text{Mg}$ , we have

to enlarge slightly the valence space used in earlier calculations. The new configurations taken now into account are those with one neutral hole in the  $2s_{\frac{1}{2}}$  shell. The reason for that is simple: The intruder configurations of  $^{31}\text{Mg}$  can be viewed as  $^{29}\text{Mg} \otimes (fp)^2$ ; and, it happens that  $^{29}\text{Mg}$  has its ground state  $\frac{3}{2}^+$  almost degenerate with  $\frac{1}{2}^+$  state dominated by this kind of configuration. We are forced to include them explicitly. This is a very peculiar situation which holds only for this nucleus. Moreover, the modification of the valence space has no appreciable consequences for nuclei other than  $^{31}\text{Mg}$ .

The resulting level scheme is plotted in Fig. 13. The correspondence with the experimental scheme is very good. From our calculation, the ground-state doublet would be  $\frac{3}{2}^+$ ,  $\frac{1}{2}^+$ , and the next excited state  $\frac{3}{2}^-$ . The  $\frac{7}{2}^-$  that the calculation places degenerate with the  $\frac{3}{2}^-$  would correspond to the experimental state at 465 keV, while the second  $\frac{3}{2}^+$  predicted at 450 keV fits with the state experimentally seen at 673 keV (see Fig. 13 for a blowup of this part of the level scheme).

As can be gathered from comparison of the experimental and theoretical level schemes of Fig. 13, many other levels are well accounted by the computation. The main failure of an  $sd$ -shell calculation, i.e., the very low density of states in the first 2 MeV of the spectrum, is completely cured by our treatment. It is worth noting here that in the best  $sd$  calculation available [32], the first excited state of  $^{31}\text{Mg}$  lies at 1.55 MeV, while our experiment places seven excited levels below this energy.

The  $^{31}\text{Mg}$  ground state comes out as a 50% mixing of normal and intruder components. The calculated  $Q_\beta$  of the decay  $^{31}\text{Na} \rightarrow ^{31}\text{Mg}$  is 15.2 MeV compared to  $Q_\beta(\text{expt}) = 15.4 \pm 0.5$  MeV.

We have computed the Gamow-Teller transition probabilities for the decay of the  $^{31}\text{Na}$  ground state to states of  $^{31}\text{Mg}$ , with the following results.

(i) The half-life of  $^{31}\text{Na}$ , computed using the bare Gamow-Teller operator, is 4 ms. With the usual renormalization, which amounts to taking  $(g_A/g_V)_{\text{eff}} = 0.77(g_A/g_V)_{\text{bare}}$ , the half-life is 7 ms, while the experi-

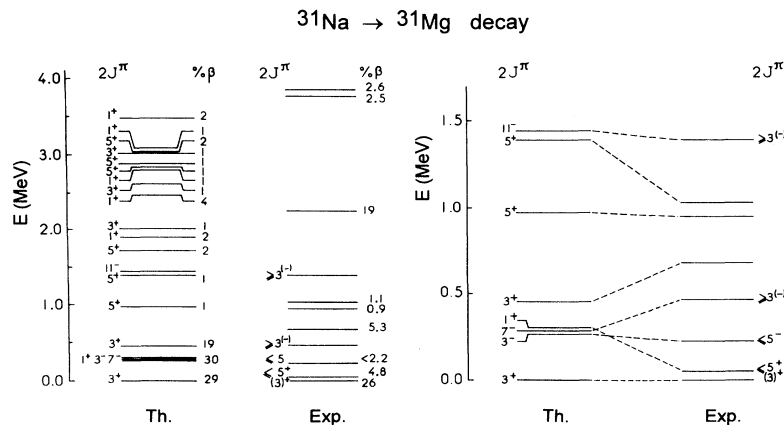


FIG. 13. Comparison of experimental and theoretical level structure of  $^{31}\text{Mg}$  and  $\beta$  intensities from the  $^{31}\text{Na}$  decay. On the right is shown a blowup of the first excited states.

mental value is 17 ms. This discrepancy may suggest that the  $^{31}\text{Mg}$  physical ground state is even more dominated by the intruder states than the one predicted by our calculation.

(ii) The fractions of beta intensity to the different  $^{31}\text{Mg}$  states are shown in Fig. 13. The agreement with the experimental  $I_\beta$  values is fair. The states at 0, 50, and 673 keV carry experimentally 26%, 8%, and 5% of the total beta intensity, while the corresponding theoretical numbers are, respectively, 29%, 30%, and 19%. The main discrepancy is the lack of calculated intensity near 2.2 MeV (6%) to cope with the 20% of beta intensity experimentally found at 2.24 MeV.

It is rather difficult to compare our results for the half-life of  $^{31}\text{Na}$  with the one of Ref. [32]. For a straightforward  $sd$ -shell calculation should produce a  $\frac{5}{2}^+$  as ground state of  $^{31}\text{Na}$ . The authors of Ref. [32] have computed the  $^{31}\text{Na}$  decay, taking the  $\frac{3}{2}^+$  excited state as if it were the ground state. However, the physical  $\frac{3}{2}^+$  ground state of  $^{31}\text{Na}$  is completely different from the  $sd$  shell  $\frac{3}{2}^+$ . Therefore a calculation of the  $^{31}\text{Na}$  decay based upon the  $sd$   $\frac{3}{2}^+$  state is not meaningful. If one plainly computes the decay of the  $sd$  ground state of  $^{31}\text{Na}$ , i.e.,  $J^\pi = \frac{5}{2}^+$ , the predicted half-life would be 2 ms instead of the 7 ms obtained in Ref. [32] for the decay of the  $\frac{3}{2}^+$ . These arguments hold not only for the half-life calculation, but also for the Gamow-Teller (GT) strength function.

The experimental values of  $B(\text{GT})$  extracted from our measurements of the  $^{31}\text{Na}$  decay, for the levels below 4 meV of  $^{31}\text{Mg}$ , are plotted in Fig. 14 by summing the strength in 200 keV bins. In the same figure are presented for comparison the predicted distributions of GT strength obtained with the  $sd + fp$  configurations. We should note that between 2.4 and 4 MeV excitation energy is  $^{31}\text{Mg}$ , some experimental strength is missing as the delayed neutron contribution has not been taken into account in this plot.

For the states populated below 2 MeV, the predicted strength exceeds the experimental value as shown in Fig. 14. This result is in agreement with the general quenching factor of experiment relative to theory which has been observed in most GT decays of  $sd$  or  $fp$  nuclei.

We have also computed the electromagnetic transitions involving the three lowest levels in  $^{31}\text{Mg}$ . The results are the following.

(i) The reduced transition probability  $\frac{1}{2}^+ \rightarrow \frac{3}{2}^+$  is  $B(M1) = 0.98 \times 10^{-2} \mu_N^2$ . Using the experimental value  $E_\gamma = 50$  keV, this gives  $\tau = 24$  ns, in agreement with our experimental result  $\tau = 23 \pm 4$  ns.

(ii) The reduced transition probability for the deexcitations of the  $\frac{3}{2}^-$  to the  $\frac{1}{2}^+$  and  $\frac{3}{2}^+$  states are

$$B(E1) [\frac{3}{2}^- \rightarrow \frac{1}{2}^+] = 0.34 \times 10^{-2} e^2 \text{fm}^2,$$

$$B(E1) [\frac{3}{2}^- \rightarrow \frac{3}{2}^+] = 0.84 \times 10^{-3} e^2 \text{fm}^2.$$

Using the experimental values for the transitions energies  $E_\gamma$ , we find a branching ratio  $\frac{66}{33}$  compared to the experimental result  $\frac{71}{29}$ .

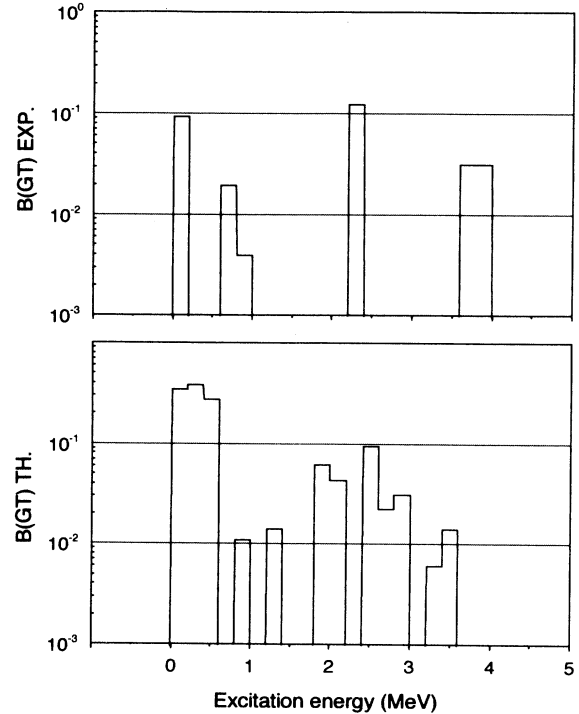


FIG. 14. Comparison of experimental (top part of the figure) and theoretical  $B(\text{GT})$  distributions in the  $^{31}\text{Na} \rightarrow ^{31}\text{Mg}$  decay plotted by summing the strengths within each 200 keV energy interval.

### B. Decay $^{31}\text{Mg} \rightarrow ^{31}\text{Al}$

The nucleus  $^{31}\text{Al}$  is a normal  $sd$ -shell nucleus. We have described it by means of a full  $sd$ -shell calculation using the USD (unified  $sd$ ) interaction of Wildenthal [33]. To the  $sd$  states we have added the intruder states without mixing. The results are the following.

(i) The  $Q_\beta$  of the decay is in our calculation 10.6 MeV

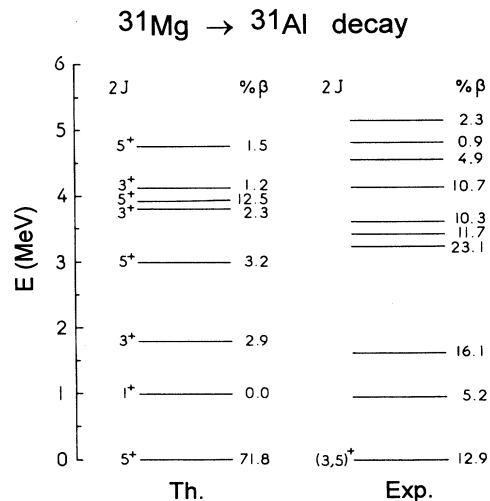


FIG. 15. Comparison of experimental and theoretical level structure of  $^{31}\text{Al}$  and  $\beta$  intensities from the  $^{31}\text{Mg}$  decay.

compared to the experimental result  $Q_\beta = 11.69 \pm 0.27$  MeV. We shall use the experimental value in the calculation of the decay properties.

(ii) The predicted half-life is 120 ms using the bare Gamow-Teller operator. With the renormalized operator, the result is  $T_{1/2} = 200$  ms compared to the experimental result  $T_{1/2}(\text{expt}) = 250$  ms. The *sd* calculation of Ref. [32] gives a half-life of 27 ms using the renormalized operator.

(iii) The calculated beta intensities are included in Fig. 15 and the Gamow-Teller strengths shown in Fig. 16. Our calculation—and also the *sd* calculation of Ref. [32]—puts too much intensity in the ground state. Nevertheless, the  $B(\text{GT})$  representation (Fig. 16) shows a general agreement between the experiment and calculations for the location of strengths, and for the first three

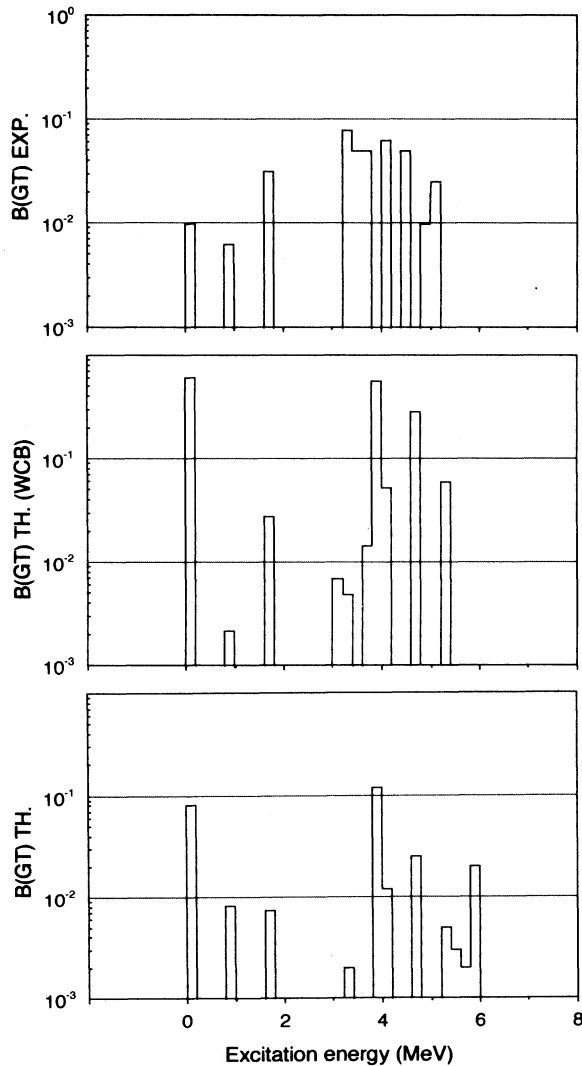


FIG. 16. Comparison of theoretical and experimental  $B(\text{GT})$  distributions in the  $^{31}\text{Mg} \rightarrow ^{31}\text{Al}$  decay: The upper part shows the experimental data, the middle part, calculations from Ref. [32], and the lower part, calculations corresponding to this work.

states the intensity is better reproduced by the inclusion of the intruder configurations.

In conclusion, for  $A = 31$  our theoretical approach improves drastically the description of the level scheme of  $^{31}\text{Mg}$ . It also explains to a large extent the existing discrepancies in the half-lives of  $^{31}\text{Na}$  and  $^{31}\text{Mg}$ . The good agreement found makes it possible to establish  $N = 19$  as the place where the transition from normal to intruder dominated ground states happens in Na, Mg, and Ne isotopes.

### C. Decay $^{32}\text{Na} \rightarrow ^{32}\text{Mg}$

In this decay parent and daughter nuclei are well inside the intruder region. The results of our calculations are as follows.

(i) The  $Q_\beta$  value is found theoretically to be 18.5 MeV, as compared to  $Q_\beta(\text{expt}) = 17.4 \pm 0.8$  MeV.

(ii) The spins  $J^\pi = 3^-$  and  $4^-$  for the ground state of  $^{32}\text{Na}$  are compatible with our calculations, which locate them, respectively, at 0 and 0.08 MeV. Therefore we have studied the  $^{32}\text{Na}$  decay for both  $J^\pi$  values of the ground state.

(iii) The calculated level scheme of  $^{32}\text{Mg}$  has the following features: The first excited state is a  $2^+$ , predicted at an excitation energy of 0.81 MeV, in full agreement with the experimental result (885 keV). Many other positive parity states are predicted, starting at 1.7 MeV excitation energy. These states have not been observed yet.

(iv) The states fed in the decay of  $^{32}\text{Na}$  are negative parity states of  $^{32}\text{Mg}$ . Experimentally, these states appear above 2.1 MeV. We have calculated them, allowing 1p-1h and 3p-3h configurations to mix. Theoretically, these states come out starting at 2.9 MeV excitation energy.

We have computed the transition probabilities for the Gamow-Teller decays to the available states in two cases, depending on the value  $J^\pi = 3^-$  or  $4^-$  for the  $^{32}\text{Na}$  parent state.

TABLE XII. Calculated  $\beta$  intensities in the decay of  $^{32}\text{Na}$ : Left part corresponds to  $J^\pi = 3^-$  for  $^{32}\text{Na}$  ground state, right part to  $J^\pi = 4^-$ .

$^{32}\text{Na}(\text{g.s.}) J^\pi = 3^-$			$^{32}\text{Na}(\text{g.s.}) J^\pi = 4^-$		
$E_x(^{32}\text{Mg})$ (MeV)	$J^\pi$	% $\beta$	$E_x(^{32}\text{Mg})$ (MeV)	$J^\pi$	% $\beta$
2.90	$3^-$	9.0	2.90	$3^-$	65.0
2.91	$2^-$	71.0			
2.95	$2^-$	6.0			
			3.17	$5^-$	1.0
			3.19	$4^-$	1.0
3.29	$3^-$	4.0	3.29	$3^-$	2.0
3.60	$3^-$	2.0	3.60	$3^-$	9.0
			3.62	$4^-$	2.0
3.73	$2^-$	3.0			
			3.96	$5^-$	4.0
			4.02	$4^-$	1.0
			4.41	$4^-$	2.0
4.48	$2^-$	1.0			
			4.79	$4^-$	1.0
5.64	$4^-$	1.0	5.64	$4^-$	2.0

In the first case  $J^\pi=3^-$ , the computed half-life is 5.4 ms using the bare Gamow-Teller operator and the experimental  $Q_\beta$  value and becomes 9.1 ms with the standard 0.77 renormalization. This result compares fairly well with the experimental half-life of 14.0 ms. The Gamow-Teller strength goes mainly to states around 3 MeV, with the intensity distribution reported in the left part of Table XII.

In the second case  $J^\pi=4^-$ , the half-life with the bare Gamow-Teller operator is 4.9 ms and with the normalized operator 8.3 ms. So no clear choice for  $J^\pi$  ( $^{32}\text{Na}$ ) can be made on this basis. The Gamow-Teller strength has the structure given by the intensity distribution reported in the right part of Table XII, which is quite similar to the structure obtained in the preceding case. If we compare with the experimental results (Table X), we see that both calculations have the same—and very

frequent—defect of predicting too much beta intensity in the few lowest states.

#### D. Concluding remarks

The new experimental results presented in this work can be adequately accounted for in a model of the region  $N=20$  far from the stability which includes in the valence space the intruder configurations obtained by promoting two  $sd$ -shell neutrons to the  $fp$  shell. To the previous experimental results establishing the existence of a region of intruder dominance at  $N=20$ , namely, the well-known spin anomaly of  $^{31}\text{Na}$  and the extremely low  $2^+$  state of  $^{32}\text{Mg}$ , one adds now the low-energy level scheme and the Gamow-Teller distribution of  $^{31}\text{Mg}$  to define  $N=19$  as the neutron number at which the transition takes place.

- 
- [1] C. Thibault, R. Klapisch, C. Rigaud, A. M. Poskanzer, R. Prieels, L. Lessard, and W. Reisdorf, *Phys. Rev. C* **12**, 644 (1975).
- [2] C. Detraz, M. Langevin, M. C. Goffri-Kouassi, D. Guillemaud, M. Epherre, G. Audi, C. Thibault, and F. Touchard, *Nucl. Phys.* **A394**, 378 (1983).
- [3] C. Detraz, D. Guillemaud, G. Huber, R. Klapisch, M. Langevin, F. Naulin, C. Thibault, L. C. Carraz, and F. Touchard, *Phys. Rev. C* **19**, 164 (1979).
- [4] B. H. Wildenthal and W. Chung, *Phys. Rev. C* **22**, 2260 (1980).
- [5] P. M. Endt, *Nucl. Phys.* **A521**, 364 (1990).
- [6] X. Campi, H. Flocard, A. K. Kerman, and S. Koonin, *Nucl. Phys.* **A251**, 193 (1975).
- [7] A. Watt, R. P. Singhal, M. H. Storm, and R. R. Whitehead, *J. Phys.* **G 7**, L145 (1981).
- [8] A. Poves and J. Retamosa, *Phys. Lett. B* **184**, 311 (1987); A. Poves, in *Proceedings of the Workshop on the Nuclear Structure of Light Nuclei Far From Stability*, Obernai, 1989, edited by G. Klotz (CRN, Strasbourg, 1991), p. 101.
- [9] P. Baumann, A. Huck, G. Klotz, A. Knipper, G. Walter, G. Marguier, H. L. Ravn, C. Richard-Serre, A. Poves, and J. Retamosa, *Phys. Lett. B* **228**, 458 (1989).
- [10] E. K. Warburton, J. A. Becker, and B. A. Brown, *Phys. Rev. C* **41**, 1147 (1990); B. A. Brown, E. K. Warburton, and B. H. Wildenthal, in *Proceedings of the Workshop on the Nuclear Structure of Light Nuclei Far From Stability* [8], p. 147.
- [11] A. Poves and J. Retamosa (unpublished).
- [12] N. Fukunishi and T. Otsuka (unpublished).
- [13] K. Heyde, in *Proceedings of the Workshop on the Nuclear Structure of Light Nuclei Far From Stability* [8], p. 129; K. Heyde and J. L. Wood, *J. Phys. G* **17**, 135 (1991).
- [14] K. Heyde, P. Van Isacker, M. Waroquier, J. L. Wood, and R. A. Meyer, *Phys. Rep.* **102**, 291 (1983).
- [15] S. K. Patra and C. R. Praharaj, *Phys. Lett. B* **273**, 13 (1991).
- [16] A. Gillibert, W. Mittig, L. Bianchi, A. Cunsolo, B. Fernandez, A. Foti, J. Gastebois, C. Gregoire, Y. Schutz, and C. Stephan, *Phys. Lett. B* **192**, 39 (1987).
- [17] D. J. Vieira, J. M. Wouters, K. Vaziri, J. R. H. Kraus, H. Wollnik, G. W. Butler, F. K. Wohn, and A. H. Wapstra, *Phys. Rev. Lett.* **57**, 3253 (1986).
- [18] N. A. Orr, W. Mittig, L. K. Fifield, M. Lewitowicz, E. Plagnol, Y. Schutz, Zhan Wen Long, L. Bianchi, A. Gillibert, A. V. Belozorov, S. M. Lukyanov, Yu. E. Penionzhkevich, A. C. C. Villari, A. Cunsolo, A. Foti, G. Audi, C. Stephan, and L. Tassan-Got, *Phys. Lett. B* **258**, 29 (1991).
- [19] X. G. Zhou, X. L. Tu, J. M. Wouters, D. J. Vieira, K. E. G. Löbner, H. L. Seifert, Z. Y. Zhou, and G. W. Butler, *Phys. Lett. B* **260**, 285 (1991).
- [20] D. Guillemaud-Mueller, C. Detraz, M. Langevin, F. Naulin, M. de Saint-Simon, C. Thibault, F. Touchard, and M. Epherre, *Nucl. Phys.* **A426**, 37 (1984).
- [21] C. L. Woods, W. N. Catford, L. K. Fifield, N. A. Orr, and R. J. Sadleir, *Nucl. Phys.* **A476**, 392 (1988).
- [22] L. K. Fifield, C. L. Woods, R. A. Bark, P. V. Drumm, and M. A. C. Hotchkis, *Nucl. Phys.* **A440**, 531 (1985).
- [23] L. K. Fifield, C. L. Woods, W. N. Catford, R. A. Bark, P. V. Drumm, and K. T. Keogh, *Nucl. Phys.* **A453**, 497 (1986).
- [24] G. Walter, P. Baumann, A. Huck, G. Klotz, A. Knipper, G. Marguier, H. L. Ravn, C. Richard-Serre, A. Poves, and J. Retamosa, in *Proceedings of the Workshop on the Nuclear Structure of Light Nuclei Far From Stability* [8], p. 85.
- [25] A. Huck, G. Klotz, A. Knipper, Ch. Miehé, C. Richard-Serre, G. Walter, A. Poves, H. L. Ravn, and G. Marguier, *Phys. Rev. C* **31**, 2226 (1985).
- [26] A. H. Wapstra and G. Audi, *Nucl. Phys.* **A432**, 1 (1985); A. H. Wapstra, G. Audi, and R. Hoekstra, *At. Data Nucl. Data Tables* **39**, 281 (1988).
- [27] G. Huber, F. Touchard, S. Bütgenbach, C. Thibault, R. Klapisch, H. T. Duong, S. Liberman, J. Pinard, J. L. Vialle, P. Juncar, and P. Jacquinet, *Phys. Rev. C* **18**, 2342 (1978).
- [28] M. Langevin, C. Detraz, D. Guillemaud-Mueller, C. Thibault, F. Touchard, and M. Epherre, *Nucl. Phys.* **A414**, 151 (1984).
- [29] G. Walter, P. Baumann, M. Bounajma, Ph. Dessagne, A.

- Huck, G. Klotz, A. Knipper, Ch. Miché, J. Rachidi, M. Ramdane, G. Marguier, C. Richard-Serre, A. Dobado, and A. Poves, in *Proceedings of the Workshop on the Nuclear Structure of Light Nuclei Far From Stability* [8], p. 71.
- [30] P. Baumann, Ph. Dessagne, A. Huck, G. Klotz, A. Knipper, G. Marguier, Ch. Miché, M. Ramdane, C. Richard-Serre, G. Walter, and B. H. Wildenthal, *Phys. Rev. C* **36**, 765 (1987).
- [31] P. Baumann, Ph. Dessagne, A. Huck, G. Klotz, A. Knipper, Ch. Miché, M. Ramdane, G. Walter, G. Marguier, H. Gabelmann, C. Richard-Serre, K. Schlösser, and A. Poves, *Phys. Rev. C* **39**, 626 (1989).
- [32] B. H. Wildenthal, M. S. Curtin, and B. A. Brown, *Phys. Rev. C* **28**, 1343 (1983).
- [33] B. H. Wildenthal, *Prog. Part. Nucl. Phys.* **11**, 5 (1983).